Plasma-surface interaction

Plasma Sources Science and Technology

PAPER

Plasma-surface interaction: dielectric and metallic targets and their influence on the electric field profile in a kHz AC-driven He plasma jet

To cite this article: A Sobota *et al* 2019 *Plasma Sources Sci. Technol.* **28** 045003

IOP Publishing Plasma Sources Science and Technology
Plasma Sources Sci. Technol. **28** (2019) 045003 (11pp) https://doi.org/10.1088/1361-6595/ab0c6a

Plasma-surface interaction: dielectric and metallic targets and their influence on the electric field profile in a kHz AC-driven He plasma jet

A Sobota[1], O Guaitella[2], G B Sretenović[3], V V Kovačević[3], E Slikboer[1,2], I B Krstić[3], B M Obradović[3] and M M Kuraica[3]

[1] Eindhoven University of Technology, EPG, Postbus 513, 5600 MB Eindhoven, The Netherlands
[2] LPP, Ecole Polytechnique, Route de Saclay, F-91128, Palaiseau, France
[3] University of Belgrade, Faculty of Physics, PO Box 44, 11001 Belgrade, Serbia

E-mail: a.sobota@tue.nl

Received 28 September 2018, revised 8 February 2019
Accepted for publication 4 March 2019
Published 4 April 2019

Abstract

Plasma catalysis, biomedical applications or atomic layer deposition at atmospheric pressure all make use of non-thermal plasmas in contact with a wide variety of surfaces. As the presence of a target (substrate) has been shown to modify the plasma in addition to the plasma modifying the target, it is reasonable to describe and study the plasma-surface as one system. This work shows how the presence of dielectric and metallic targets influences a kHz AC-driven discharge in a He plasma jet. Next to bringing the absolute values of the axial electric field along the plume of the jet, the presence of the surface has been shown to significantly elongate both the plume and the electric field profile. In addition, when a dielectric target is placed closer than the maximum length of the freely expanding jet, the electric field profile is enhanced only in the vicinity of the dielectric, typically between 0.3 and 2 mm above the target surface. The maximum measured relative increase is 31%, for 1000 SCCM flow with the target at 7 mm distance, when the electric field increased from 14.1 kV cm^{-1} for the freely expanding jet to 32.6 kV cm^{-1} when the jet was impinging on glass. Finally, a grounded metallic target enhances the electric field compared to the glass target only within a very thin layer just above the surface, typically about 0.2 mm. The highest measured electric field was 40.1 kV cm^{-1} at a grounded metallic target 12 mm away from the nozzle, for 1000 SCCM of helium flow. The discussion on the effects of the flow on the electric field profile are supported by the visualization of the flow. The discussion brings, among other, the comparison of properties between the 30 kHz AC-driven system and the 5 kHz pulsed jet.

Keywords: electric field, discharge, atmospheric pressure plasma jet, helium, Stark, target, dielectric

1. Introduction

Non-thermal atmospheric pressure plasma jets are very small plasma sources that opened up new application possibilities in a grand way. Unlike classical atmospheric- and high-pressure discharges (e.g. arcs), the non-thermal property of these discharges can be kept in such imbalance that the heavy particle temperature can stay close to 300 K. Combined with a rich chemistry when operating in combination with room air, as well as the simplicity and low costs of manufacturing, possibilities from the usage in medicine to plasma catalysis and atomic layer deposition on temperature-sensitive surfaces with a whole spectrum between appeared.

Based on the classical streamer theory, the inner workings of the kHz-driven version of the plasma jet are explained by the rapid progression of fast ionization waves. The fast ionization wave is characterized by the separation of charge that causes a locally high electric field, which causes ionization in front of itself, which in turn causes more separation of charge [1]. The electric field is, thus, what propagates with the fast ionization wave, not the produced particles. It is also one of the fundamental properties of the fast ionization wave that determines its other properties, such as speed. Although it is key for understanding fast ionization waves and thus the fundamentals of plasma jets as well, until a few years ago this quantity was beyond the reach of experimental research.

With the development of applications of plasma jets, it became clear that the produced discharge, being very small and highly transient, is severely influenced by the presence of any foreign object in its vicinity [2–5]. For example, the presence of a target influences the abundance of species in the plume of the plasma jet, e.g. OH radicals [6, 7], or the He metastable density [8, 9]. Furthermore, when interacting with a target, it is the electrical properties of the target that determine the behaviour of the discharge. Low-permittivity targets induce a surface discharge [10–15], while high-permittivity and high-conductivity targets at times induce return strokes [11, 16–20].

It is therefore necessary to study the plasma jets in the same environment in which they are going to be applied. This is important for the applications (e.g. the knowledge of the electric fields applied on a living person during treatment with a plasma jet is useful for the assessment of risks) and for the understanding of the plasma alike.

This work brings the measurements of electric fields in the gas phase of a plasma jet when the jet interacts with a target. Solid targets of different electrical properties were used: glass without a ground plane in its vicinity, glass with a ground plane on its back side and a grounded metallic target. The gas flow speed is varied as well. The results clearly show that the targets in combination with the flow speed have an influence on the electric field values, but also profile.

2. Experimental details

The experiments were performed on an atmospheric pressure plasma jet described in [10, 22]. As shown on the left-hand side of figure 1, the setup consists of a high voltage electrode that also serves as gas inlet (inner diameter 0.8 mm, outer diameter 1.6 mm) housed in a Pyrex capillary (inner diameter 2.5 mm, outer diameter 4 mm). The high voltage electrode is powered by a sinusoidal signal at 30 kHz with 2 kV amplitude (4 kV peak to peak). The grounded electrode is a brass ring 3 mm wide, grounded via a 1 kΩ resistor. The grounded electrode was at 5 mm distance from the charged electrode throughout the study. Under these circumstances there is exactly one ionization wave per voltage period expelled from the capillary into the room atmosphere, in the positive half-cycle of the period, as described in [22]. Due to the relatively low voltage, without the presence of a target the power

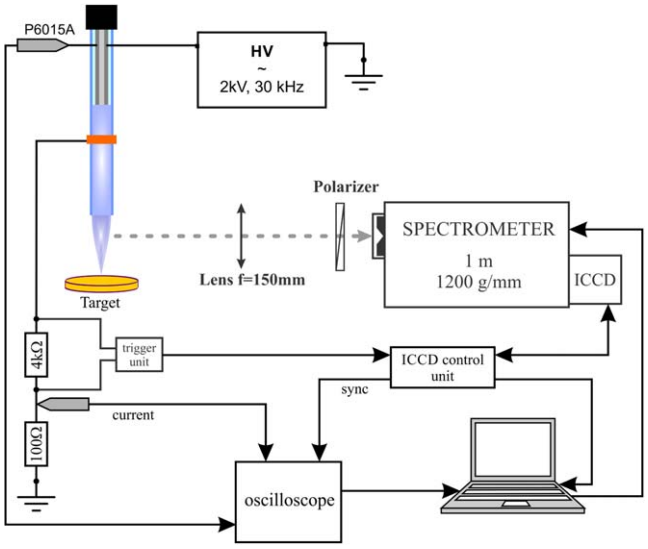

Figure 1. The experimental setup. Modelled after the figures in [21–24].

dissipated in the plasma is 0.2 W, without the occurrence of microdischarges. The jet was operated vertically, the direction of the gas flow pointing downwards. The flow of Helium is varied from 700 SCCM to 2000 SCCM, corresponding to the range between 2.4 and 6.8 m s^{-1} in this setup.

Three targets were used in the experiments. The first target was 2 mm thick glass, the second target had a grounded metallic layer on the back side of the glass (the side that was not in contact with the plasma) and the third target was grounded metal in contact with the plasma.

Exactly like in the previously published studies on the same plasma system [24–26], the electric field values were measured using optical emission spectroscopy on a forbidden line of Helium (2^1P–4^1F), through the observation of its position in the spectrum with respect to the closest allowed line at 492.19 nm (2^1P–4^1D). The method is based on the work of Foster [27] and well described in more recent publications [28–30]. The electric field strength value can be determined from the distance between the allowed and the forbidden Helium line and is given by the formula [31]:

$$E\,(\mathrm{kVcm^{-1}}) = (-58.557 + 18.116\Delta\lambda_{FA} + 3130.96\Delta\lambda_{FA}^2 + 845.6\Delta\lambda_{FA}^3)^{0.5}, \quad (1)$$

where $\Delta\lambda_{FA}$ is the shift of the peak of the forbidden Helium line from the allowed line at 492.19 nm.

The spectroscopy setup is schematically shown on the right-hand side of figure 1. The 1 m Solar MSDD 1000 imaging spectrometer with 1200 grooves mm^{-1} grating was used in combination with the iCCD Princeton Instruments PI-MAX2 camera with a 1024 × 1024 px CCD as a detector. The plasma plume was imaged on the slit of the spectrometer using an achromatic lens with the focal length of 150 mm, achieving a 1:1 object-image projection. A polarizer was used at the slit in order to transmit only π-polarized light. Consequently, we only measure the axial electric field component. The opening of the slit was kept at 70 μm. The spatial resolution was 12.5 μm $pixel^{-1}$, and the spectral resolution was

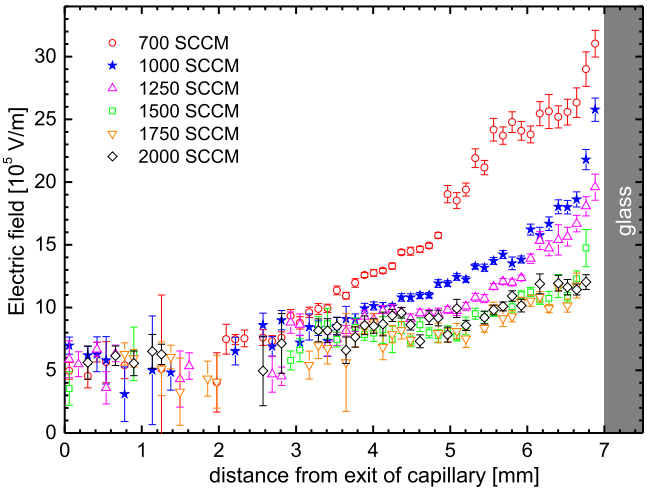

Figure 2. Electric field profiles for different flows of He as a function of the distance from the exit of the capillary. The measurements were taken at 30 kHz, 2 kV amplitude (4 kV_{pp}). Glass target was used at 7 mm distance from the exit of the capillary.

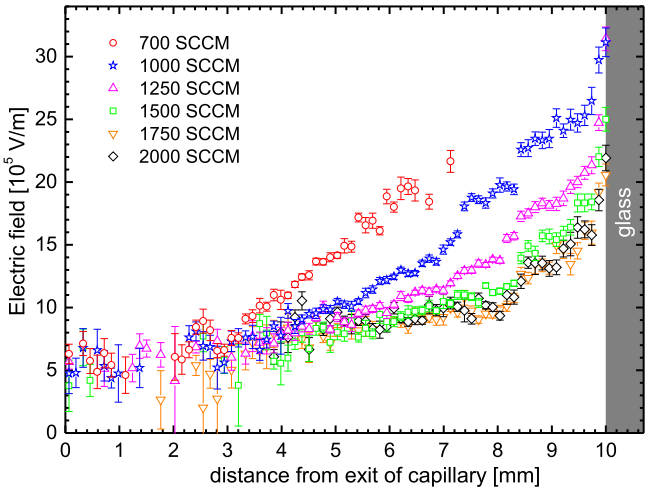

Figure 3. Electric field profiles for different flows of He as a function of the distance from the exit of the capillary. The measurements were taken at 30 kHz, 2 kV amplitude (4 kV_{pp}). Glass target was used at 10 mm distance from the exit of the capillary.

0.010 8 nm $pixel^{-1}$. The measurements were obtained with 90 accumulations and 100 000 expositions per accumulation.

The Schlieren images of the gas flow was obtained using the setup in detail described in [24, 26], based on [32]. The images were taken with the blade at the focal point of the second lens with an exposure time for every image of 33 μs, i.e. one voltage period.

3. Results and comparison to existing work

3.1. Electric field measurements

Figures 2 and 3 show the electric field profile along the axis of the plume for different flows, for the glass target at 7 mm and 10 mm respectively. The differences between the profiles for different gas flows, but without a target, were observed and discussed previously [24], where it was proposed that the mixing of Helium with the surrounding air was the reason for the different behaviour at different flows. The higher concentration of air in the flow for lower Helium flow speeds caused the plume to constrict closer to the nozzle and the electric field to rise faster as the ionization wave travelled away from the nozzle. Still, even though the electric field rose faster for lower flows, the maximum value was approximately constant at 1.7×10^6 V m^{-1}. The maximum field dropped below that value only in the conditions where the plasma caused the gas flow to become turbulent, which was above 1750 SCCM, or 5.95 m s^{-1}.

The presence of the glass target (figures 2 and 3) causes the electric field profile to change. Like in the freely expanding jet [24], the electric field values rose with the distance from the nozzle, with the maxima at the target surface. When the target was at 10 mm from the nozzle, the plasma plume did not reach it for the lowest flow.

However, unlike with the freely expanding jets, when a target was present at different flows, the electric field profiles

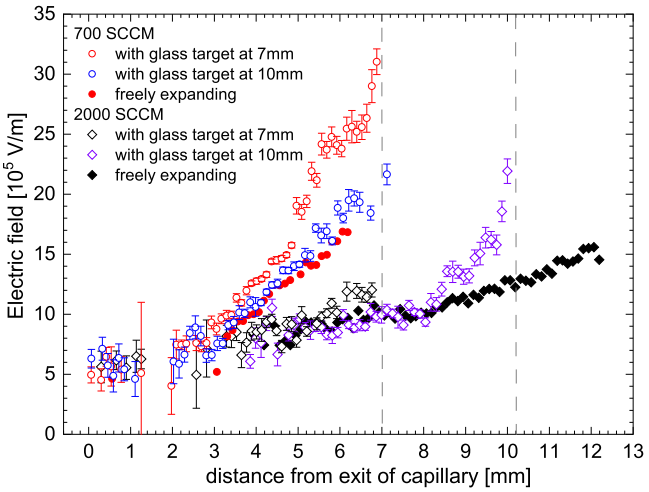

Figure 4. Electric field profiles as a function of the distance from the exit of the capillary. The measurements were taken at 30 kHz, 2 kV amplitude (4 kV_{pp}). Glass target was used at 7 and 10 mm for He flows at 700 SCCM and 2000 SCCM. The positions of the targets are indicated by dashed lines.

showed different maxima, the highest being for the lowest flow. In figure 2, where the glass target was at 7 mm from the nozzle, plasmas reached the target for all flows. At 700 SCCM (2.4 m s^{-1}) the maximum is at 3.1×10^6 V m^{-1}, which is approximately double when compared to the freely expanding jet [24], as shown in figure 4. The electric field maxima lower with the increase of the flow, to 2.6×10^6 V m^{-1} for 1000 SCCM (3.4 m s^{-1}) and 2.0×10^6 V m^{-1} for 1250 SCCM (4.2 m s^{-1}). The maxima for higher flows are at 1.2×10^6 V m^{-1} at the target, which is lower than the maxima in the freely expanding jet, but still a bit higher than the electric field values at the distance of 7 mm in the freely expanding jet (1.0×10^6 V m^{-1} at 1500 SCCM —2000 SCCM). A resembling effect with similar electric field values has been observed using the same jet in the same

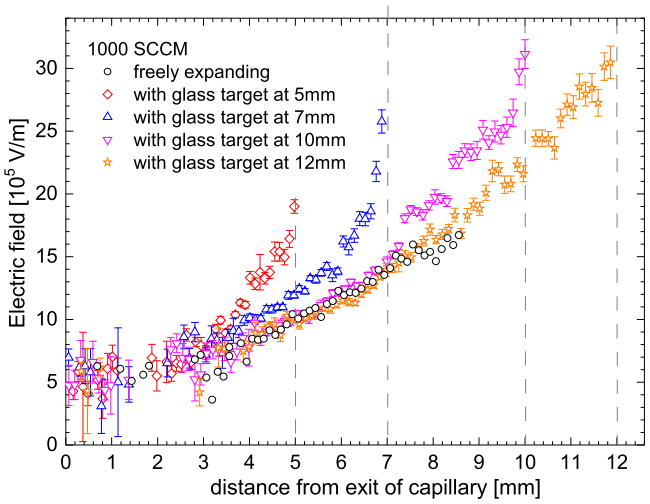

Figure 5. Electric field profiles as a function of the distance from the exit of the capillary. The measurements were taken at 30 kHz, 2 kV amplitude (4 kV_{pp}). Glass target at different distances was used (5 , 7 , 10 and 12 mm) at a single He flow of 1000 SCCM. The positions of the targets are indicated by dashed lines.

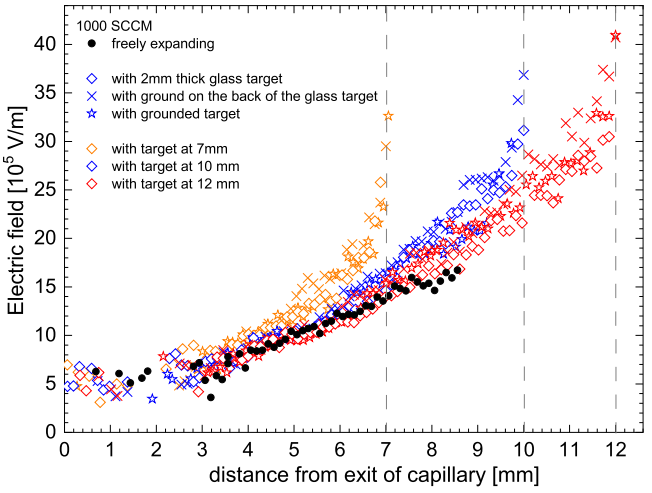

Figure 6. Electric field profiles as a function of the distance from the exit of the capillary. The measurements were taken at 30 kHz, 2 kV amplitude (4 kV_{pp}). Three different targets were used (glass, glass with a metallic layer at the back side and grounded metal) at distances of 7, 10 and 12 mm from the exit of the capillary at a single He flow of 1000 SCCM. The positions of the targets are indicated by dashed lines. Error bars were omitted for better readability of the graph. Like in other graphs, the error bars are the largest very close to the capilary, where the electric field is the lowest, and just next to the surface of the target.

experimental setup, but with a liquid (water, saline) target [26].

In the case where the target was 10 mm away, the ionization waves at 700 SCCM Helium flow did not reach the target, however the maximum electric field in the profile is 2.2×10^6 V m^{-1}, which is higher than in the freely expanding jet, see figures 3 and 4. In addition, even though the ionization waves did not reach the target, the electric field profile is longer than the one in the freely expanding jet suggesting a longer plasma plume. The maximum at both 1000 SCCM and 1250 SCCM is at 3.1×10^6 V m^{-1}, while the maxima of 1500 SCCM, 1750 SCCM and 2000 SCCM are lower (2.5×10^6 V m^{-1}, 2.2×10^6 V m^{-1} and 2.1×10^6 V m^{-1} respectively), but still higher than in the freely expanding jet.

As it is evident that discharges at different flows exhibit different behaviour when interacting with the target, for a clear comparison figure 4 shows the electric field profiles for two extreme flows—700 SCCM and 2000 SCCM, with the targets at 7 and 10 mm away from the nozzle, compared to the data for the freely expanding jet, published in [24]. The lower flow caused the target to have a much larger influence on the electric field profile with respect to the freely expanding jet. A similar effect has been observed in the same discharge in [26], where water was used as target, and where the electric field profile at the flow of 2000 SCCM was not visibly affected by the presence of the target, except for the fact that it ended at the water surface.

Figure 5 shows the electric field profile for a single flow speed of 1000 SCCM (3.4 m s^{-1}) for targets at 5, 7, 10 and 12 mm away from the nozzle, compared to the electric field profile for the freely expanding jet. From the profile with the target at 12 mm it is visible that the presence of the target extended the plume length by 30% in this case. In that case the electric field profile is also a clear extension of the profile of the freely expanding jet. The target, however, always causes a steep increase of electric field just above the target surface. The maximum of the electric field rose as the target got further away from the nozzle, and it is at 1.9×10^6 V m^{-1}, 2.6×10^6 V m^{-1}, 3.1×10^6 V m^{-1} and 3.1×10^6 V m^{-1} for the glass target at 5, 7, 10 and 12 mm, respectively. The graph also shows that the effect of the target on the electric field profile, in particular the sharp rise of the electric field values, happens only very close to the target, approximately in the last 0.3 mm before the target.

Figure 6 shows the electric field profiles for three different targets—glass, glass with ground on the back side and grounded plate—for a single flow of 1000 SCCM (3.4 m s^{-1}) and three different distances of the targets, 7, 10 and 12 mm. The comparison is given with the electric field profile in the freely expanding jet. The data for all three types of targets are bundled together to demonstrate that there is very little difference in the electric field profiles between these three targets along the whole profile, except for the very near vicinity to the surface. This observation is not intuitive due to large differences in electrical properties between e.g. a glass target with no metallic surface in its vicinity and a grounded surface. The observation was, however, reproduced for all the targets and all the target positions. It is worth noticing that the grounded targets did cause higher electric fields than the ones consisting only of glass. Table 1 gives the values of the electric field measured closest to the target for all conditions. Unless the last measurement point is relatively far away from the target (given in red in the table), as a rule the grounded target gives rise to the highest electric field strength at the target, and the glass target without metal in its vicinity to the lowest electric field strength. The difference between these two extremes can be as large as 1×10^6 V m^{-1}.

Table 1. The electric field measured closest to the target in all conditions, from data in figure 6. If a very close measurement point is missing, the distance and the electric field value are given in red. *T*1 is glass target, *T*2 glass target with grounded metal on the back side and *T*3 is the grounded metallic target. *E* denotes the electric field strength in 10^6 V m^{-1}, while dft means *distance from target*, expressed in mm.

Position of target	*T*1		*T*2		*T*3	
	E	dft	*E*	dft	*E*	dft
7 mm	2.6	0.12	3.0	0	3.3	0.14
10 mm	3.1	0	3.7	0	3.0	0.27
12 mm	3.0	0.14	3.8	0.28	4.1	0

There is a limited number of articles available, mostly results of simulations, that have the electric field data for comparison with this work. The simulation that bears the most similarity with this jet configuration is [33], where a jet of the same dimensions and configuration was used on a dielectric target of $\epsilon_r = 4$, 1cm away, at the flow of 1 SLM, but using fast voltage pulses rather than AC-driven powered electrode. Under those conditions the electric field at the target was determined at 3.0–3.5$\times 10^6$ V m^{-1}. This is in good agreement with our value in the same condition on glass (3.1×10^6 V m^{-1}). A study from 2015 [11] had targets of $\epsilon_r = 2$ and metal at 7.5 mm from the nozzle and the electric fields at the target were 2.2×10^6 V m^{-1} and 2.8×10^6 V m^{-1} respectively. This constitutes a 27% increase of the electric field when metal was used instead of low-permittivity dielectric, which corresponds perfectly to the measured increase in this work at 7 mm distance. Finally, in the work [34] the simulated electric field at the metallic grounded target was 3.5×10^6 V m^{-1} when the target was 5 mm away from the nozzle, which is somewhat higher than obtained in this work. Except for the absolute values, trends from simulations are reproduced as well, where a metallic grounded target does show a higher electric field in the gas phase than when a dielectric target is used.

3.2. Visualization of flow

Figure 7 visualizes the flow for two different flow speeds (1000 SCCM and 2000 SCCM), for a freely expanding jet as well as for a jet-target system with a glass target at different distances. The two flow speeds were chosen because they represent some of the parameters from the measurements of the electric fields. In addition, from previous measurements [24] it was known that when the plasma is on, the 1000 SCCM He flow speed still produces a laminar flow, while at 2000 SCCM the flow develops vortices some millimeters from the nozzle. Similar results were obtained in [35] as well.

It can be observed that the presence of the target influences the structure of the flow. In the case of the lower flow, the presence of the target causes the flow to go through a stagnation zone, to eventually turn into flow parallel to the surface of the target. After a distance of 10–15 mm, the buoyancy force acting on He causes the flow to change direction and the part of the flow impinging on the target surface to constrict for all distances of the target. In combination with the fact that in the experiment the jet and the target surface were not perfectly perpendicular, the flow becomes asymmetric.

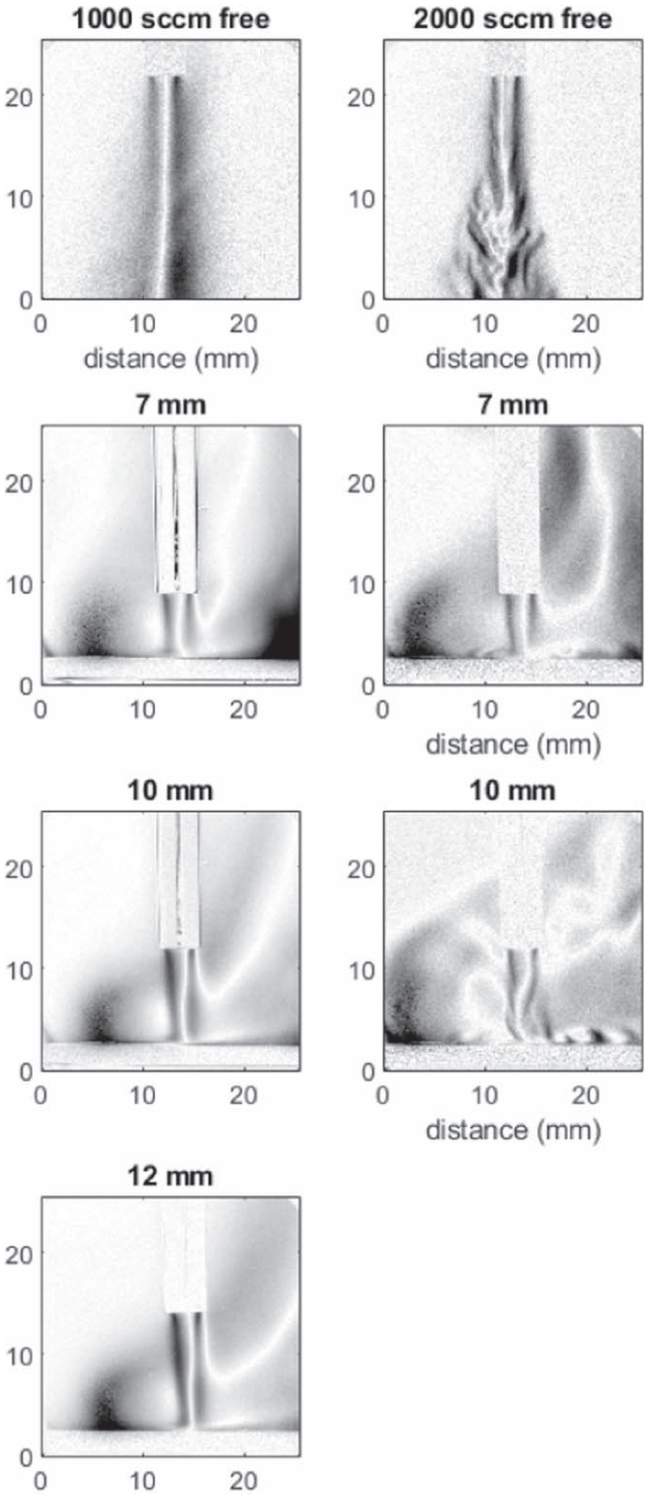

Figure 7. The visualization of the flow for two different flow speeds (1000 SCCM and 2000 SCCM) in a freely expanding jet and with a glass target at different distances. Flow visualization of freely expanding jets was shown in [26].

In the case of the higher flow, the images show that the distance between the nozzle and the target surface is a very sensitive parameter for the structure of the flow. When the target is placed within the part of the flow that is still partly laminar (7 mm away in this case), the central part of the flow is affected only minimally. When the target is further away, in the zone close to where the vortices in the freely expanding jet start to form, the presence of the target significantly potentiates the formation of vortices in the flow. The direct comparison will be available in the Discussion section.

3.3. In summary:

- the plume length is significantly elongated when the target is placed at a further distance than the maximum length of the freely expanding plume
- when a dielectric target is placed closer than the maximum length of the freely expanding jet, the electric field profile is enhanced only in the vicinity of the dielectric, typically between 0.3 and 2 mm above the target surface.
- a grounded target enhances the electric field only within a very thin layer just above the surface, typically about 0.2 mm.
- for a flow that is laminar in a freely expanding jet, the presence of the target induced a constriction of the flow as it reached the target, for distances of 7 mm or above.
- in a flow that turns from partially laminar to turbulent in a freely expanding jet, the position of the target is sensitive, as it can induce the appearance of vortices earlier in the flow.

4. Discussion

4.1. Gas flow

Figures 2–4 show that at a given position, the presence of the target has a larger influence on the electric field profile for lower flows. In combination with the data for the freely expanding jet [24], these figures also show that if the target is placed approximately in the first half of the visible plasma plume of the freely expanding jet, the electric field profile remains unaffected by the presence of a glass target. This is the case at 1500 SCCM, 1750 SCCM and 2000 SCCM (visible plume lengths of the freely expanding jet are 15.3 mm, 15.5 mm and 15.5 mm respectively) for the target placed at 7 mm away from the capillary.

Figure 5 shows that for a single flow, shifting the target further away can extend the electric field profile by 30%. The further the target, the higher the maximum electric field. Still, the increase of the electric field happens only close to the target, otherwise the values are similar to those of the freely expanding jet.

These results can be discussed through the influence of the gas mixing on the electric field profile, but also the influence of the electrical properties of the target. Here the gas flow will be discussed.

The flow with the plasma on in this work is laminar except for the highest flow, 2000 SCCM, as shown in figure 7 and already demonstrated in [24, 26]. The gas composition obtained in [24] is similar to the results of Raman scattering giving the air density for 1500 SCCM He in this same system, but using ns pulses to drive the discharge instead of the AC signal at 30 kHz [15].

In [24] it has already been shown that the gas mixing is the cause of the stretch of the electric field profile in the freely expanding jet in increasing flows. By using simulations of gas composition for different He flows, it has been suggested that the electric field values are connected to a specific mixture of He in the ambient air, the maximum measured electric field in that work (approximately 1.7×10^6 V m^{-1}) being at 0.014 air molar fraction for all flows if the flow is in a laminar regime while the plasma is on. It should be noted that the gas composition was calculated for the flow without the plasma, therefore neglecting the effects of the plasma on the flow. As it has been reported many times [35–47], the plasma affects the laminar length of the flow and it is conceivable that it also alters its composition. Still, the underlying cause of the maximum electric field being a function of the air fraction is the lowering of the effective Townsend ionization coefficient with the increase of air admixture, therefore requiring a higher electric field for the same electron production rate.

The large effect of the target on the electric field profile in the low flows and its negligible effect in the high flows is most probably caused by the compression of the electric potential lines against the boundary between the air and the target at low flows, as argued in [18, 26]. At high flows there is no visible contraction of the jet on the surface of the target, causing the volume in which the ionization wave propagates to remain unchanged by the presence of the surface. In other words, the purity of the He flow reaching the target remains high enough to not reach the roughly 1% of entrained air at which the electric field seems to be strongly affected.

This is supported by the results of flow visualization. For an easier comparison several images were made (figure 8) where the flow of the freely expanding jet was overlaid on the flow while plasma was on, with a glass target at different positions. Focusing first on the lower flow, at 1000 SCCM the top two images in the figure show that the flow is altered by the presence of the target under the jet. Already at the distance of 7 mm, there is contraction of the flow above the target, suggesting a difference in the gas mixing with respect to the freely expanding jet. The effect is even more pronounced for the case of a distant target at 12 mm. In line with this, the electric field was found to increase at the target at this flow.

A quantitative measurement of the He/air fraction was not done for this system in the conditions at which the electric field was measured, however it is possible to make an estimate based on the behaviour of the effective first Townsend ionization coefficient as a function of He/air fraction and reduced electric field, as presented in [24]. The conditions at 1000 SCCM—1500 SCCM flow speed were chosen for this because the flow is laminar, thus the calculations of gas composition from [24] can be taken as representative. The procedure was to (i) take the α_{eff} belonging to the electric

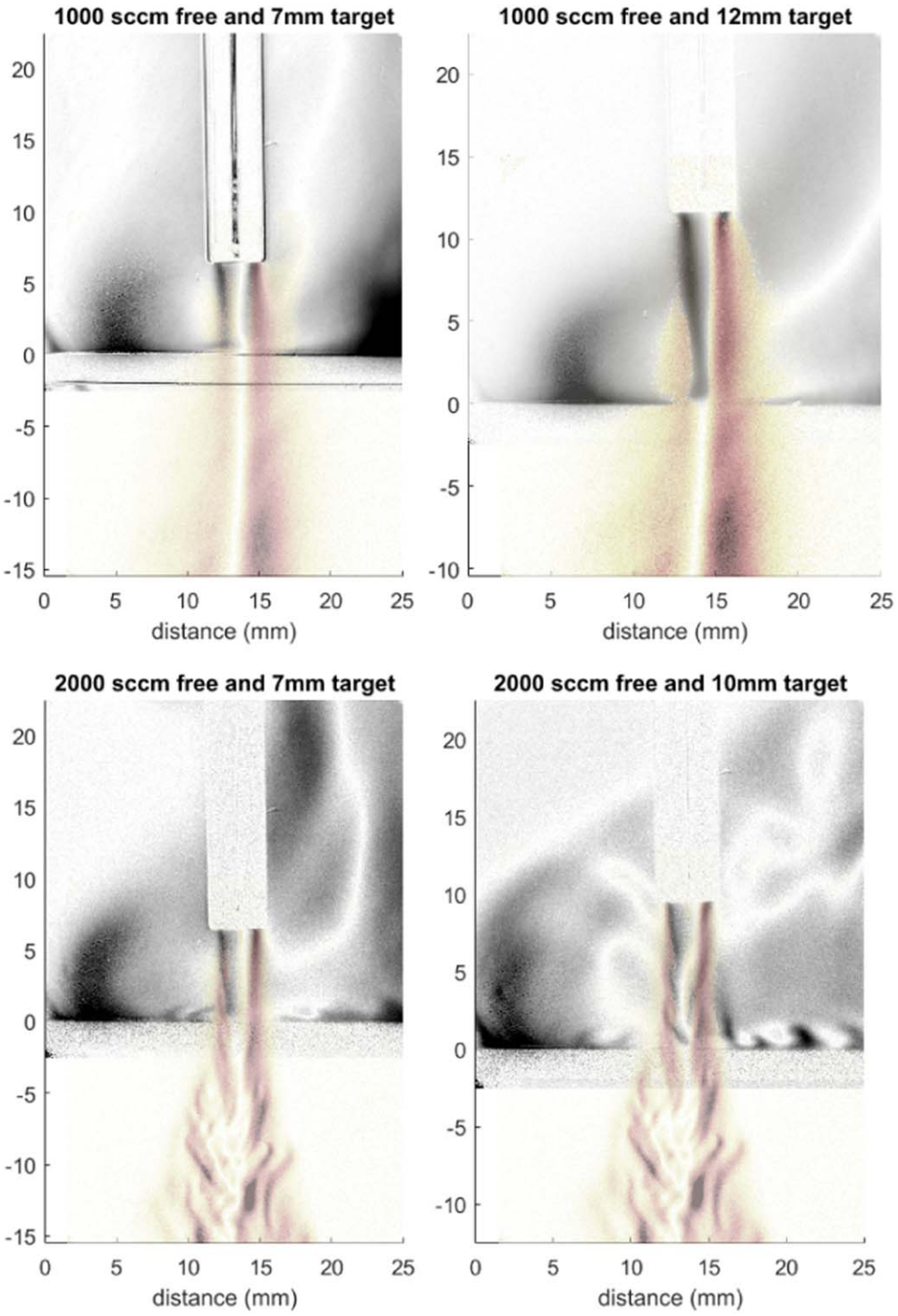

Figure 8. The comparison of the structure of flow between the freely expanding jet and the plasma jet with a glass target in front of it, for 1000 SCCM and 2000 SCCM He flow. The images were made by overlaying the relevant images of flow. The flow with a target is shown in grayscale, while the flow of the freely expanding jet is given in colour. The plasma was always on.

field measured and gas composition calculated at 5, 10 and 12 mm distance from the nozzle for a freely expanding jet; (ii) take the electric field values for the same conditions, but with a glass target present; (iii) look for the He/air fraction for the electric fields with the target present, at which the α_{eff} would be the same as in the freely expanding jet in the same position in space. In this way a very rough estimate can be made of the influence of the target on the gas mixing in the area just above the target. The results are presented in table 2. From the condition of matching α_{eff} at a given point in space, the gas mixing induced by the target has significant influence on the gas composition, lowering the He fraction to under 80% in some cases. The comparison between the visualized flow of the freely expanding jet and the experiments with the target

Table 2. The He/air molar fraction calculated for a freely expanding jet 24] and roughly estimated from the condition of an equal effective first Townsend ionization coefficient for a jet impinging on a glass target. 'Free' designates the values for He/air fraction of the freely expanding jet at the point where the target would be (5, 7, 10 mm), while 'target' stands for the values just above the target when the target is present. The results are presented for three speeds of He flow: 1000, 1250 and 1500 SCCM.

Position of target	1000 SCCM		1250 SCCM		1500 SCCM	
	Free	Target	Free	Target	Free	Target
5 mm	0.998	0.85				
7 mm	0.993	0.79	0.997	0.83	0.998	0.895
10 mm			0.988	0.74	0.993	0.824

present in figure 8 shows contraction of the He channel and vortex structures around it, making the reduced He/air ratio plausible.

The highest He flow used in this work is 2000 SCCM. Under the conditions when the plasma is on at this speed the flow becomes turbulent several millimeters away from the nozzle. In the bottom two images in figure 8 a comparison is given between the freely expanding jet and a jet with a target in front of it for two target distances. At 7 mm, the target is in the part of the flow where the vortices still have not developed and the flow is still partially laminar. In this condition there is very little influence of the target on the flow. When the target is at 10 mm, its presence causes vortices in the flow to start developing closer to the nozzle, therefore altering the flow. Both these effects are also visible in the electric field profile (figure 4). At 7 mm distance, there is a minuscule increase of the electric field close to the target, within the error bars compared to the freely expanding jet. At 10 mm, the electric field profile is significantly altered.

Following the description of the flow structure (as described for this jet in [10]), there is a stagnation point in the flow, located just above the surface of the target, where the flow approaching the surface divides into different counter-flowing streams. In some cases an increased amount of He could be expected at the stagnation point when compared to the freely expanding jet. This could mean a locally lower electric field. This effect is, however, only expected when the target is placed very close to the nozzle, or when the flow is fast enough to generate a significant stagnation zone [48]. Figure 8 shows that a target as close as 7 mm away already causes the constriction of the flow at 1000 SCCM just above the surface of the target, possibly because of the buoyancy force that acts upon He, causing it to form vortices at approximately 5 mm away from the impact point. In addition, the jet and the target are in practice never perfectly perpendicular to each other, nor with respect to gravity. In conculsion, even though the stagnation region is present in the flow of the jet-target system, the local increase of He just above the target is not something that is expected unless the target is very close to the nozzle because of imperfections in experiments and because of the buoyancy force acting on He.

4.2. Electrical properties of the target

The electrical properties of the target have influence on the electric field profile at 1000 SCCM, as shown in figure 6 and table 1. The transition from the glass target to the grounded target caused the increase of the maximum measured electric field by 27% for the target at 7 mm and by 37% for the target at 12 mm. These assessments of increase should, however, be taken only as indications, as the measurements could not be taken exactly at the same place, and taking into account the fast rise of the electric field close to the target, a small shift in the spatial coordinate can mean a large error. The increase of 30% is expected, according to [11], when comparing the maximum electric field for the grounded target to glass. In addition, the absolute values of the electric field from modelling studies [11, 33, 34] fit well with the measured values in this campaign.

The most important reason for the smaller increase of the electric field on a glass target with respect to the grounded target, or glass with ground on the other side, in this set of experiments is probably the larger compression of the equipotential lines when the ground is in vicinity of the ionization wave propagating in the effluent of the plasma jet, as visible from modelling studies (e.g. [11]). When comparing the results with a glass target and a glass target with the ground on the back side, we can exclude the effect of a different chemistry, different produced species or different species forming surface charge, as in both cases the jet interacts with the same material—glass.

The presence of a metallic target does cause a difference in the behaviour of the discharge in the vicinity and on the target surface, as previously demonstrated and outlined in the introduction. A low-permittivity target typically induces surface ionization waves, while metallic targets cause at least one return stroke to develop. This also means that there is enough charge density in the charged channel to sustain a return stroke in the case of a metallic target, which was demonstrated for a jet in this geometry, but driven by pulsed voltage [15]. In that work the electron density at the metallic target was shown to be more than twice as large when compared to the case with the glass target. The fact that in this work we observe a higher electric field just above the surface of the grounded target when compared to glass is in line with those previous findings.

The elongation of the plasma plume when a target is present, even if it is a glass target with low-permittivity, might be caused by different gas mixing like discussed above, but it is probable that this is also an electrical effect of the target. The presence of a dielectric material, even with low-permittivity, has been shown to modify the dynamics with which the fast ionization waves travel [49–55]. The dielectric does not even have to be in the path of the ionization wave to modify its trajectory, it only has to be in its close vicinity [56]. There are several explanations offered for this phenomenon. One is that the presence of the dielectric modifies the electric potential lines at its surface, thus modifying the local electric field [50–53, 55–61]. As the Townsend ionization coefficient is a steep function of the reduced electric field [1], this local

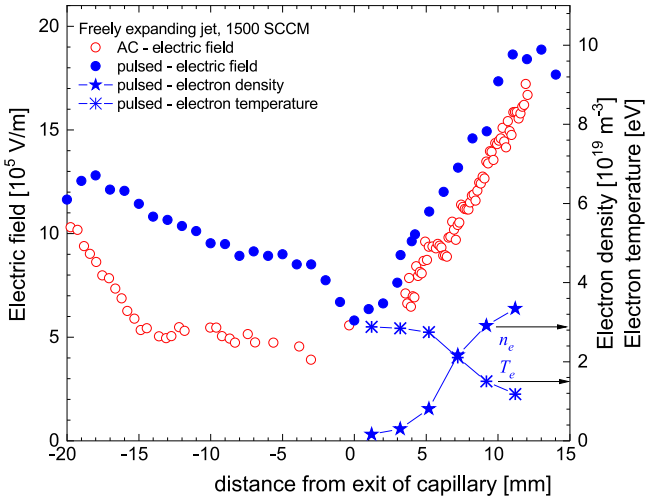

Figure 9. The comparison between the plasma jet configuration used in this work, driven by AC kHz sine voltage at 30 kHz (in red) [24, 25], and the same configuration driven by positive voltage pulses at 5 kHz repetition frequency, 6 kV amplitude, 1 μs length and 50 ns risetime (in blue) [15, 73]. Electric field profiles are shown as a function of the distance from the exit of the capillary. Negative values denote that the electric field was measured in the capillary of the jet. Electron density and temperature for the pulsed jet are scaled on the right axis. The gas flow speed was 1500 SCCM and all data shows properties of the freely expanding jet.

modification is an important parameter. However, many authors agree that the effects of dielectrics on discharge development cannot be explained only by the local modification of the electric field in the vicinity of the dielectric [62–64]. Many have argued that the dielectric surface serves as storage of charge deposited by previous discharges. In this way it causes a 'memory effect' on the surface. It has been shown, for example, that the speed of surface discharges on low-permittivity dielectrics is the biggest for pre-deposited charge of the opposite polarity [65–68]. The charge can be emitted from the surface by photoemission of electrons [51–53, 69–71] or negative ion detachment [54, 72].

One argument in this direction comes from the results of imaging for the jet used in this work impinging on a glass surface, published in [10]. As the ionization wave was approaching the target, a discharge has already formed on the target before the ionization wave had reached it. This was evidenced through light emission from the target. This suggests that the glass surface does store a certain amount of charge leftover from previous discharges, and it is possible that the discharge that pre-forms on the surface as the ionization wave approaches it is one of the causes of the elongation of the plasma plume when a target is present.

4.3. Differences and similarities between AC- and pulse-driven jets

The work published up to this point on this plasma jet can be divided in two groups—the AC-driven jet at 30 kHz and 2 kV amplitude [24–26] and the pulse-driven jet using pulses of 50 ns rise time, at 5 kHz and 4–6 kV [15, 33, 73]. The comparison of properties for the freely expanding jet at 1500 SCCM flow of Helium is shown in figure 9. The original data has been published in [15, 24, 25, 73]. Error bars have been omitted for clarity. The comparison for the jet in the presence of a low-permittivity dielectric target looks very similar and is for that reason not shown.

The electric field measurements can be compared. The profiles look very similar and the values are close, especially in the plume. The values are, however, systematically larger in the pulsed system. The smallest difference is approximately 2–3 kV cm^{-1}, in the plasma plume.

Even though the electric field profile seems similar, the visual appearance of the AC and pulsed jet, as well as their electron properties are different. The plume of the pulsed jet is much thinner and several times longer, while the electron densities are 1–2 orders of magnitude larger in the pulsed jet (electron density for the AC jet has been estimated in [25] but not measured).

The fact that the axial electric fields in the plasma plume are relatively close in value and the electron densities have been estimated to be different by at least an order of magnitude can in fact be supported by the basics of discharge physics. The ionization process that governs most of the properties of every ionization wave can be expressed through the first ionization coefficient [1], which is an exponential function of the reduced electric field. In Helium with 1% air admixture, as shown in [24], this ionization coefficient will increase by 2 orders of magnitude for the ionization distance of 1 mm and the increase of electric field from 15 to 17 kV cm^{-1} at atmospheric pressure. At the distance of 0.1 mm it will increase by a factor 2 instead. Even if the ionization distance is not known, it is reasonable to expect significantly lower electron densities in the AC-driven system even if the electric field strength is only 2–3 kV cm^{-1} lower.

Why is the electric field systematically larger in the pulsed system? The crucial detail is that, when using AC voltage at 30 kHz, the voltage changes very slowly, and one voltage period takes 33 μs, which is orders of magnitude slower than the breakdown event necessary to initiate a discharge [1]. Consequently, discharges in the AC work are initiated at the breakdown voltage, lower than the applied 2 kV amplitude. In contrast, jets driven by nanosecond pulses can easily be made at an overvoltage, e.g. at 6 kV for this same system [15]. This essential difference is a likely cause for a significantly larger electric field close to the electrode system (in the capillary, as shown in figure 9) and somewhat larger in the plasma plume.

Another contribution to the difference is caused by the difference in the repetition frequency, 30 kHz in the AC case and 5 kHz in the pulsed system. According to [74, 75], where negative ions left over after discharges at different frequencies were measured, 30 kHz is a high enough frequency to have significant density of negative ions remaining from one period to another, which could be a source of seed electrons to be obtained by photodetachment in front of the positive ionization front. This makes the required electric field (and thus ionization coefficient) for the propagation of the fast ionization wave smaller, while at 5 kHz there is less charge available, thus requiring a higher electric field for

propagation. The cited work refers to measurements where jets were characterized by using a mass spectrometer, thus the results may be mostly comparable to the conditions where the jet impacts on a metallic target.

5. Conclusions

This work examined the interaction of an AC-driven atmospheric pressure plasma jet in He with solid targets of different electrical properties—from glass to a grounded metallic target—through the influence of the electric field in the plume. The two main conclusions can be summarized as follows:

(i) The presence of a target in the vicinity of the plasma jet significantly influences the electric field profile compared to the jet freely expanding in air. Even the low-permittivity target (glass) without metallic objects in its vicinity causes the electric field profile to be modified close to the target to values almost double when compared to the freely expanding jet. The cause for this is most probably the compression of the potential lines in the presence of the air-target interface as well as spatial compression of the ionization wave, due to gas mixing in the presence of a target. At high gas flows, when the target does not cause the spatial collapse of the He channel, this effect is not observed.

(ii) The permittivity and the conductivity of the target have influence on the maximum electric field measured in the plume, exhibiting approximately 30% increase for the grounded target in comparison to glass. This increase fits well with the predictions from simulations.

Acknowledgments

AS, VK and GS would like to thank the European Cooperation in Science and Technology Action COST TD1208 for the financial support for a short-term scientific mission. GS, IK, VK, BO and MK would like to thank the Ministry of Education and Science of the Republic of Serbia for financial support through Project 171034 and Project 33022.

ORCID iDs

A Sobota https://orcid.org/0000-0003-1036-4513
O Guaitella https://orcid.org/0000-0002-6509-6934
G B Sretenović https://orcid.org/0000-0003-4817-4723
V V Kovačević https://orcid.org/0000-0002-8575-1668
E Slikboer https://orcid.org/0000-0002-7716-907X
B M Obradović https://orcid.org/0000-0002-3221-7779

References

[1] Raizer Y P 1991 *Gas Discharge Physics* (Berlin: Springer)
[2] Zaplotnik R, Bišćan M, Krstulović N, Popović D and Milošević S 2015 *Plasma Sources Sci. Technol.* **24** 054004
[3] Yan W and Economou D J 2016 *J. Appl. Phys.* **120** 123304
[4] Akishev Y S, Karalnik V B, Medvedev M A, Petryakov A V, Trushkin N I and Shafikov A G 2017 *J. Phys. Conf. Ser.* **927** 012051
[5] Akishev Y S, Karalnik V B, Medvedev M A, Petryakov A V, Trushkin N I and Shafikov A G 2017 *J. Phys. Conf. Ser.* **927** 012040
[6] Yonemori S and Ono R 2014 *J. Phys. D: Appl. Phys.* **47** 125401
[7] Riès D, Dilecce G, Robert E, Ambrico P F, Dozias S and Pouvesle J M 2014 *J. Phys. D: Appl. Phys.* **47** 275401
[8] Urabe K, Morita T, Tachibana K and Ganguly B N 2010 *J. Phys. D: Appl. Phys.* **43** 095201
[9] Zaplotnik R, Bišćan M, Popović D, Mozetič M and Milošević S 2016 *Plasma Sources Sci. Technol.* **25** 035023
[10] Guaitella O and Sobota A 2015 *J. Phys. D: Appl. Phys.* **48** 255202
[11] Norberg S A, Johnsen E and Kushner M J 2015 *J. Appl. Phys.* **118** 013301
[12] Wang L, Zheng Y and Jia S 2016 *Phys. Plasmas* **23** 103504
[13] Abuzairi T, Okada M, Bhattacharjee S and Nagatsu M 2016 *Appl. Surf. Sci.* **390** 489–96
[14] Prysiazhnyi V, Ricci Castro A H and Kostov K G 2017 *Braz. J. Phys.* **47** 65–71
[15] Klarenaar B L M, Guaitella O, Engeln R and Sobota A 2018 *Plasma Sources Sci. Technol.* **417** 257–69
[16] Gerling T, Nastuta A V, Bussiahn R, Kindel E and Weltmann K D K D 2012 *Plasma Sources Sci. Technol.* **21** 034012
[17] Hu J T, Wang J G, Liu X Y, Liu D W, Lu X P, Shi J J and Ostrikov K 2013 *Phys. Plasmas* **20** 083516
[18] Norberg S A, Johnsen E and Kushner M J 2016 *J. Phys. D: Appl. Phys.* **49** 185201
[19] Darny T, Pouvesle J M, Puech V, Douat C, Dozias S and Robert E 2017 *Plasma Sources Sci. Technol.* **26** 045008
[20] Viegas P, Péchereau F and Bourdon A 2018 *Plasma Sources Sci. Technol.* **27** 025007
[21] Sobota A, Guaitella O and Garcia-Caurel E 2013 *J. Phys. D: Appl. Phys.* **46** 372001
[22] Sobota A, Guaitella O and Rousseau A 2014 *Plasma Sources Sci. Technol.* **23** 025016
[23] Sretenović G B, Krstić I B, Kovačević V V, Obradović B M and Kuraica M M 2014 *J. Phys. D: Appl. Phys.* **47** 102001
[24] Sobota A, Guaitella O, Sretenović G B, Krstić I B, Kovačević V V, Obrusník A, Nguyen Y N, Zajíčková L, Obradović B M and Kuraica M M 2016 *Plasma Sources Sci. Technol.* **25** 065026
[25] Sretenović G B, Guaitella O, Sobota A, Krstić I B, Kovačević V V, Obradović B M and Kuraica M M 2017 *J. Appl. Phys.* **121** 123304
[26] Kovačević V V, Sretenović G B, Slikboer E, Guaitella O, Sobota A and Kuraica M M 2018 *J. Phys. D: Appl. Phys.* **51** 065202
[27] Foster J S 1927 *Proc. R. Soc.* A **117** 137–63
[28] Kuraica M M and Konjević N 1997 *Appl. Phys. Lett.* **70** 1521–3
[29] Kuraica M, Konjević N and Videnović I 1997 *Spectrochim. Acta* B **52** 745–53
[30] Obradović B M, Ivković S S and Kuraica M M 2008 *Appl. Phys. Lett.* **92** 191501
[31] Cvetanović N, Martinović M M, Obradović B M and Kuraica M M 2015 *J. Phys. D: Appl. Phys.* **48** 205201

[32] Settles G S 2001 *Schlieren and Shadowgraph Techniques* (Berlin: Springer) (https://doi.org/10.1007/978-3-642-56640-0)
[33] Viegas P, Slikboer E, Obrusník A, Bonaventura Z, Sobota A, Garcia-Caurel E, Guaitella O and Bourdon A 2018 *Plasma Sources Sci. Technol.* **27** 094002
[34] Yan W and Economou D J 2017 *J. Phys. D: Appl. Phys.* **50** 415205
[35] Boselli M, Colombo V, Ghedini E, Gherardi M, Laurita R, Liguori A, Sanibondi P and Stancampiano A 2014 *Plasma Chem. Plasma Process.* **34** 853–69
[36] Oh J S, Olabanji O T, Hale C, Mariani R, Kontis K and Bradley J W 2011 *J. Phys. D: Appl. Phys.* **44** 155206
[37] Jiang N, Yang J, He F and Cao Z 2011 *J. Appl. Phys.* **109** 093305
[38] Ghasemi M, Olszewski P, Bradley J W and Walsh J L 2013 *J. Phys. D: Appl. Phys.* **46** 052001
[39] Robert E, Sarron V, Darny T, Riès D, Dozias S, Fontane J, Joly L and Pouvesle J M 2014 *Plasma Sources Sci. Technol.* **23** 012003
[40] Foletto M, Puech V, Fontane J, Joly L and Pitchford L C 2014 *IEEE Trans. Plasma Sci.* **42** 2436–7
[41] Whalley R D and Walsh J L 2016 *Sci. Rep.* **6** 31756
[42] Qaisrani M H, Xian Y, Li C, Pei X, Ghasemi M and Lu X 2016 *Phys. Plasmas* **23** 063523
[43] Xian Y B, Hasnain Qaisrani M, Yue Y F and Lu X P 2016 *Phys. Plasmas* **23** 103509
[44] Zheng Y, Wang L, Ning W and Jia S 2016 *J. Appl. Phys.* **119** 123301
[45] Darny T, Pouvesle J M, Fontane J, Joly L, Dozias S and Robert E 2017 *Plasma Sources Sci. Technol.* **26** 105001
[46] Babaeva N Y, Naidis G V, Panov V A, Wang R, Zhao Y and Shao T 2018 *Phys. Plasmas* **25** 063507
[47] Borghei S M, Vaziri N and Alibabaei S 2018 *J. Phys. Conf. Ser.* **992** 012005
[48] Satti R P and Agrawal A K 2006 *Int. J. Heat Fluid Flow* **27** 336–47
[49] Shimazaki T and Tsuneyasu I 1990 *IEEE Trans. Electr. Insul.* **25** 1161–9
[50] Abdel-Salam M, Weiss P and Lieske B 1992 *IEEE Trans. Electr. Insul.* **27** 309–19
[51] Allen N and Ghaffar A 1995 Propagation of positive streamers over insulating surfaces in air *Proc. 1995 Conf. Electr. Insul. Dielectr. Phenom.* (Piscataway, NJ: IEEE) pp 447–50
[52] Elizondo J, Krogh M, Smith D, Stoltz D, Wright S, Sampayan S, Caporaso G, Vitello P and Tishchenko N 1997 Vacuum surface flashover and high pressure gas streamers *Dig. Tech. Pap. 11th IEEE Int. Pulsed Power Conf. (Cat. No.97CH36127)* vol 2 (Piscataway, NJ: IEEE) pp 1027–32
[53] Allen N and Mikropoulos P 1999 *IEEE Trans. Dielectr. Electr. Insul.* **6** 357–62
[54] Akyuz M, Gao L, Cooray V, Gustavsson T, Gubanski S and Larsson A 2001 *IEEE Trans. Dielectr. Electr. Insul.* **8** 902–10
[55] Pritchard L and Allen N 2002 *IEEE Trans. Dielectr. Electr. Insul.* **9** 371–80
[56] Sobota A, Lebouvier A, Kramer N J, Van Veldhuizen E M, Stoffels W W, Manders F and Haverlag M 2009 *J. Phys. D: Appl. Phys.* **42** 015211
[57] Abdel-Salam M and Weiss P 1992 *IEEE Trans. Electr. Insul.* **27** 320–33
[58] Faircloth D and Allen N 2003 *IEEE Trans. Dielectr. Electr. Insul.* **10** 285–90
[59] Allen N, Tan B and Rodrigo H 2008 *IEEE Trans. Dielectr. Electr. Insul.* **15** 390–8
[60] Tan B, Rodrigo H and Allen N 2008 *IET Sci. Meas. Technol.* **2** 196–207
[61] Sobota A, van Veldhuizen E and Stoffels W 2008 *IEEE Trans. Plasma Sci.* **36** 912–3
[62] Blaise G and Le Gressus C 1991 *J. Appl. Phys.* **69** 6334–9
[63] Li C R and Sudarshan T S 1994 *J. Appl. Phys.* **76** 3313–20
[64] Trusov K K 2010 *J. Phys. D: Appl. Phys.* **43** 065201
[65] Fouracre R A, Santos E, Timoshkin I, Given M J and Macgregor S J 2006 Surface discharge propagation: the influence of surface charge *Conf. Rec. 2006 27th Int. Power Modul. Symp.* (Piscataway, NJ: IEEE) pp 39–42
[66] Santos E, Fouracre R and MacGregor S 2004 Discharge velocity effects across charged insulator surfaces *17th Annu. Meet. IEEE Lasers Electro-Optics Soc. 2004. LEOS 2004.* (Piscataway, NJ: IEEE) pp 675–8
[67] Deng J, Matsuoka S, Kumada A and Hidaka K 2010 *J. Phys. D: Appl. Phys.* **43** 495203
[68] Celestin S, Canes-Boussard G, Guaitella O, Bourdon A and Rousseau A 2008 *J. Phys. D: Appl. Phys.* **41** 205214
[69] Allen N and Faircloth D 2003 *IEEE Trans. Dielectr. Electr. Insul.* **10** 295–304
[70] Jorgenson R E, Warne L K, Neuber A A, Krile J, Dickens J and Krompholtz H G 2003 Effect of dielectric photoemission on surface breakdown: An LDRD Report *{SANDIA} Report* Sandia National Laboratories, Albuquerque, New Mexico
[71] Timatkov V V, Pietsch G J, Saveliev A B, Sokolova M V and Temnikov A G 2005 *J. Phys. D: Appl. Phys.* **38** 877–86
[72] Allen N L and Hashem A A R 2002 *J. Phys. D: Appl. Phys.* **35** 2551–7
[73] Hofmans M and Sobota A 2019 *J. Appl. Phys.* **125** 043303
[74] Oh J S, Aranda-Gonzalvo Y and Bradley J W 2011 *J. Phys. D: Appl. Phys.* **44** 365202
[75] McKay K, Oh J S, Walsh J L and Bradley J W 2013 *J. Phys. D: Appl. Phys.* **46** 464018